Sensitivity of Simulated Ammonia Fluxes in Rocky Mountain National Park to Measurement Time Resolution and Meteorological Inputs

Lillian E. Naimie¹, Da Pan¹, Amy P. Sullivan¹, John T. Walker², Aleksandra Djurkovic², Bret A. Schichtel^{3,4}, Jeffrey L. Collett, Jr.¹

Abstract. Gaseous ammonia (NH₃) is an important precursor for secondary aerosol formation and contributes to reactive nitrogen deposition. NH₃ dry deposition is poorly-rarely quantified due to the complex bidirectional nature of NH₃ atmosphere-surface exchange and lack of high time-resolution in situ NH₃ concentration and meteorological measurements. To better quantify NH₃ dry deposition, measurements of NH₃ were made above a subalpine forest canopy in Rocky Mountain National Park (RMNP) and used with in situ micrometeorology to simulate bidirectional fluxes. NH₃ dry deposition was largest during the summer, with 4748% of annual net NH₃ dry deposition occurring in June, July, and August. A net annual dry deposition estimated using measured 30 minute NH₃ concentrations and in situ meteorological data, accounted for 6% of total RMNP reactive inorganic N deposition. Because in situ, high_-time_-resolution concentration and meteorological data are often unavailable, the impacts impact on estimated deposition from utilizing more commonly available biweekly NH₃ measurements and ERA5 meteorology wereinput data was evaluated. Fluxes simulated with biweekly NH₃ concentrations, commonly available from NH₃ monitoring networks, underestimated NH₃ dry deposition by 4529%. These fluxes were strongly correlated with 30-minute fluxes integrated to a biweekly basis (R² = 0.8889) indicating that a correction factor could be applied to mitigate the observed bias. Application of an average NH₃ diel concentration pattern to the biweekly NH₃ concentration data removed the observed low bias. Annual NH₃ dry deposition from fluxes simulated with reanalysis meteorological inputs exceeded simulations using in situ meteorology measurements by a factor of 2.59%.

1. Introduction

Gaseous ammonia (NH_3) is an important atmospheric constituent, with effects on atmospheric chemistry and the nitrogen cycle. Atmospheric deposition of reactive nitrogen (N_r) is linked to nitrogen oxides (NO_x) and NH_3 emissions. Emissions of NO_x and NH_3 have many potential fates including chemical transformation, dry deposition, particle formation, and wet deposition. Anthropogenic emissions of NO_x and NH_3 are produced predominantly by combustion and agriculture, respectively

¹Department of Atmospheric Science, Colorado State University, Fort Collins, CO 80523, USA

²United States Environmental Protection Agency, Office of Research and Development, Durham, NC 27709, USA

³Cooperative Institute for Research in the Atmosphere, Colorado State University, Fort Collins, CO 80523, USA

⁴US National Park Service, Air Resource Division, Lakewood, CO 80225-0287, USA

¹⁰ Correspondence to: Jeffrey L. Collett, Jr. (collett@colostate.edu)

(Walker et al., 2019a), although there are also NH₃ emissions from traffic, wastewater treatment, and wildfires (Tomsche et al., 2023; Walker et al., 2019b). Due to increased food demand and industrialization, anthropogenic N_r has been increasing annually (Galloway et al., 2008; Kanakidou et al., 2016). Excess reactive nitrogen deposition has well-documented adverse effects on ecosystem health including lake—eutrophication, soil acidification, decreased biodiversity, and increased N in freshwater bodies (Baron, 2006; Bobbink, 1991; Boot et al., 2016; Holtgrieve et al., 2011; Pan et al., 2021; Zhan et al., 2017). As a result of effective NO_x emission controls, the balance of N_r wet deposition across the US has shifted from oxidized N-dominated to reduced N-dominated, and dry deposition of NH₃ at times dominates total N_r deposition (Driscoll et al., 2024; Li et al., 2016, Walker et al., 2019a). The National Emission Inventory (NEI) indicates that US NO_x emissions were reduced by 46% between 2013 and 2023, while NH₃ emissions increased by 13% (US EPA, 2023).

Critical loads, deposition levels below which harmful effects are not expected to occur, have been estimated for many ecosystems (e.g. Bowman et al., 2012; Schwede and Lear, 2014). In Rocky Mountain National Park (RMNP), a critical load of 1.5 kg N ha⁻¹ yr⁻¹, based on wet deposition of NO₃⁻ and NH₄⁺, has been established to avoid adverse effects on the ecosystem (Baron, 2006). The pre-industrial nitrogen load has been estimated at 0.2 kg N ha⁻¹ yr⁻¹ while the current wet deposition rate is as high as 3.65 kg N ha⁻¹ yr⁻¹, approximately 15x the natural background and significantly higher than the critical load (Benedict et al., 2013a; Burns, 2003; CDPHE, 2007). Although the RMNP N_r critical load only considers wet deposition of NO₃⁻ and NH₄⁺, dry deposition can also contribute significantly to total N_r deposition. NH₃ dry deposition in RMNP was estimated to be the third largest contributor to total N_r deposition, accounting for 18% of N_r deposition from November 2008 to November 2009 (Benedict et al., 2013a).

NH₃ dry deposition, however, remains a highly uncertain component of N_r deposition, and fluxes are rarely measured (Walker et al., 2019b). Previous studies in RMNP have estimated NH₃ dry deposition using unidirectional inferential models, where the NH₃ deposition velocity (V_d) was approximated as 70% of the HNO₃ deposition velocity (Beem et al., 2010; Benedict et al., 2013a; Benedict et al., 2013b) and NH₃ emission from the surface was ignored. In reality, NH₃ exchange between the atmosphere and surface is bidirectional, including deposition to and emission from the surface (Sutton et al., 1995). Several models have been developed to simulate the bidirectional exchange of NH₃ with the surface (Massad et al., 2010; Pleim et al., 2013; Zhang et al., 2010). Key model inputs include micrometeorology, soil and vegetation parameters, and atmospheric concentrations. In practice, fluxes can change quickly and even reverse direction with changing environmental conditions. Gaseous NH3 is challenging and expensive to measure at high time resolution; lower-cost weekly or biweekly passive diffusion-based sampler measurements are more commonly utilized for long-term monitoring (Butler et al., 2016; Hu et al., 2021; Li et al., 2016; Schiferl et al., 2016). Previous efforts have used these low-cost measurements to quantify NH3 dry deposition (Shen et al., 2016; Tanner et al., 2022; Walker et al., 2008). Detailed, high_-time_-resolution meteorological observations at the location of interest are also desired when estimating dry deposition. Due to the frequent unavailability of such data, reanalysis meteorological data is often used as a substitute (Schrader et al., 2018; Wichink Kruit et al., 2012). Schrader et al. (2018) investigated the impact of low time-resolution NH₃ concentrations on modeled fluxes. They found that using monthly NH3 concentrations underestimates total NH3 dry deposition. However, due to a linear relationship between 65 simulations using monthly NH₃ concentrations and those using hourly NH₃ concentrations, they were able to generate a site-specific correction to compensate for the use of low time-resolution concentration data. Simulations were done using a simplified parameterization of the bidirectional exchange model described in Massad et al. (2010) and the NH₃ concentrations were simulated using the LOTOS-EUROS model (Hendricks et al., 2016).

Understanding and managing these biases could unveil opportunities to estimate NH₃ deposition when high_-time_-resolution, in situ concentration, and meteorological observations are unavailable. Using high_-time_-resolution NH₃ concentration measurements, we provide the first estimate of NH₃ annual dry deposition to an RMNP forest canopy using a bidirectional exchange model driven by high_-time_-resolution NH₃ concentration data and in situ micro-meteorological measurements. We use in situ data collected in RMNP to determine if site-specific correction factors suggested by Schrader et al. (2018) apply to real-world observations and whether correction factors can be employed to reduce biases associated with NH₃ simulations using lower-cost, low_-time_-resolution NH₃ measurements such as those available from the U.S. Ammonia Monitoring network (AMoN) (Puchalski et al., 2011). We also tested if an average NH₃ diel pattern could be applied to reduce these biases and, if so, the length of measurements necessary to adequately describe the diel pattern. Finally, we examine biases introduced by substituting reanalysis meteorological data for high_-time_-resolution in situ measurements.

2 Data and methods Methods

2.1 Site locationLocation

Study observations were collected in RMNP in northern Colorado. The park, established to preserve the natural landscape, including montane, subalpine, and alpine ecosystems, is predominantly above 3000 m where ecosystems developed under nutrient-deprived conditions and are therefore sensitive to excess inputs of nitrogen. Nitrogen deposition has been a historical problem in RMNP; with diatom changes documented starting in the 1950s and more recent effects including eutrophication and changes to plant species (Baron, 2006; Baron et al., 2000; Korb and Ranker, 2001).

The area east of RMNP (Fig. 1) includes a large urban corridor and extensive agricultural activity in the plains. The Front Range urban corridor, spanning from Denver to Fort Collins, is a major source of nitrogen oxide emissions (Benedict et al., 2013b). The northeast plains of Colorado are predominantly agricultural and include major sources of NH₃ emissions from both animal feeding operations and crop production. The spatial pattern seen for feedlots is broadly consistent with the spatial distribution of other agricultural activities. Pan et al. (2021) found that 40% of summertime dry deposition of NH₃ in RMNP was associated with transport from agricultural regions to the east.

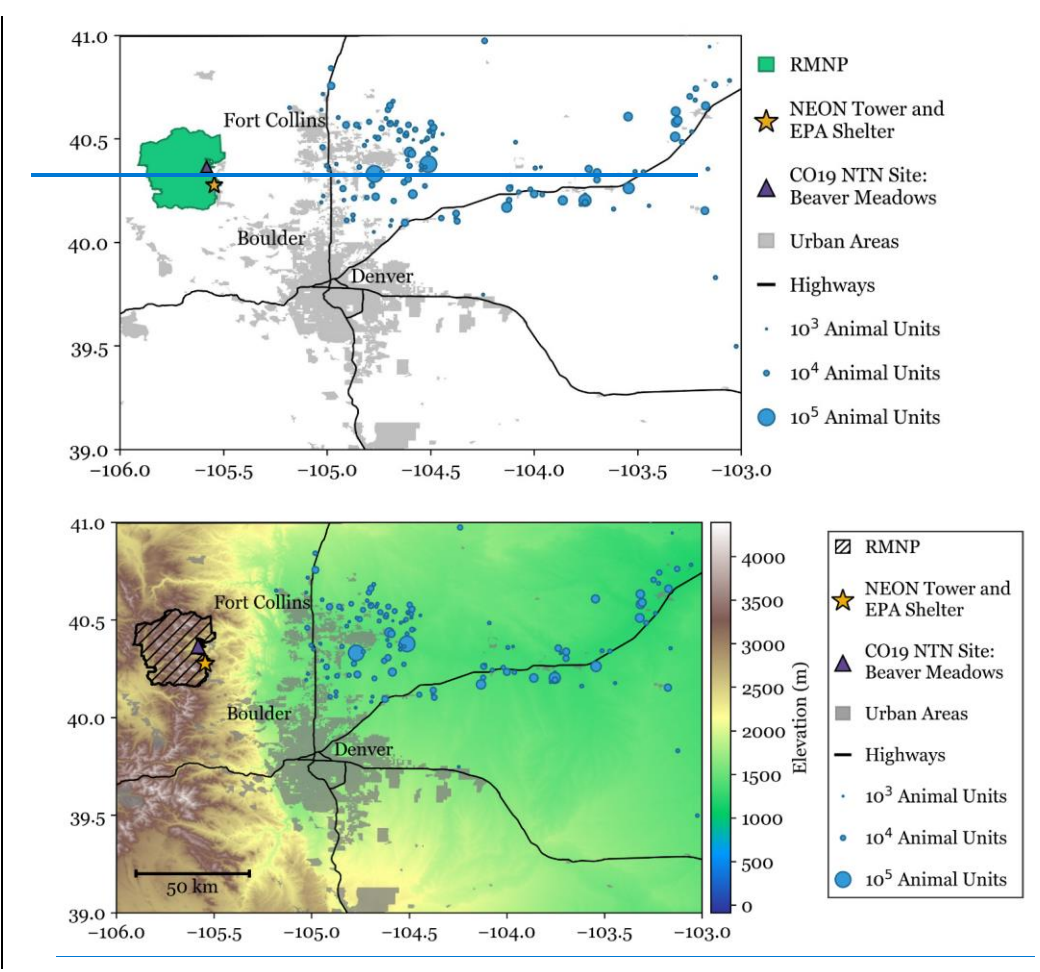


Figure 1. A map of the study region. Animal units are shown as the number of permitted animals as of 2017, scaled by an animal unit factor relative to the species. Elevation data is from the US Geological Survey Global Multi-resolution Terrain Elevation Data 2010 (GMTED2010) at 7.5-arc-second spatial resolution, or 225 m (available at: https://earthexplorer.usgs.gov/).

Data was collected at two adjacent locations for this study, both near the base of Longs Peak in Rocky Mountain National Park: a National Ecological Observatory Network (NEON) tower site (40.275903, -105.54596) and a nearby National Park Service shelter (~500 m north of the NEON tower), from September 2021 through August 2022. The study location, denoted

with a star in Fig. 1, is 2750 m above sea level. The tower is surrounded by lower montane forest, comprised of predominantly evergreen needleleaf species, including ponderosa pine, juniper, and Douglas fir. There are also groves of quaking aspen located in the region. Meteorological transport to the site is generally bimodal. Prevailing downslope transport from the northwest occurs generally overnight and during the cooler months, when ammonia concentrations are typically low. The mountain-plains circulation generates daytime upslope transport, bringing air masses from the plains east of the park up into RMNP. This pattern strengthens during warmer seasons. Periods of synoptically forced sustained upslope transport are also common, especially during spring and autumn (Gebhart et al., 2011). Downslope and upslope transport patterns are not due west and east at the study site because of channellingehanneling by local topography.

At RMNP₃ a diel pattern in ambient NH₃ concentrations has commonly been observed in past measurements. This pattern is primarily driven by changes in transport patterns that carry NH₃ emissions to the park (Benedict et al., 2013b; Juncosa Calahorrano et al., 2024) and, sometimes, modified by changes in the atmosphere-surface exchange of NH₃, especially during NH₃ uptake and emission from dew formation and evaporation (Wentworth et al., 2016).

Meteorological and soil data were accessed from the RMNP NEON flux tower. The mean canopy height in the area surrounding the tower is 19 m. Temperature (mean = 6 °C), relative humidity (mean = 40 °e), and annual days of precipitation

2.2 Micrometeorological measurements Measurements

2.2.1 in situ micrometeorology Micrometeorology

are highly variable at the site due to its high elevation. Mean values were calculated from September 2021 to September 2022. Snowfall typically occurs between October and May. The seasonal mean temperatures (relative humidities) are as follows: winter (December, January, and February) mean is -3 °C (30%), spring (March, April, and May) mean is 2 °C (44%), the summer (June, July, and August) mean is 15 °C (49%), and the fall (September, October, and November) mean is 8 °C (37%). 120 Precipitation is measured at 1-minute resolution by a Belfort AEPG II 600M weighing gauge. Precipitation events were defined as periods of rainfall separated by at least one hour without precipitation. During our study period, there were 27 precipitation events in the winter, 62 in the spring, 63 in the summer, and 26 in the fall. Meteorological data accessed from the NEON site includes wind vectors, frictionfrictional velocity, Obukhov length, soil temperature, short wave radiation, relative humidity, air density, air pressure, and air temperature above the tree canopy. The 125 meteorological observations used from the NEON tower are 30-minute mean values. Direct measurements of wind vectors, air temperature, short wave radiation, relative humidity, air density, and air pressure were used from the tower-top measurements (25 m-agl). 3D wind vectors were measured at 20 Hz using the CSAT-3 sonic anemometer (Campbell Scientific Inc., Logan, Utah, USA). Soil temperature was taken as the average across 5 collection sites within 200 m of the flux tower. Leaf area index (LAI) is estimated at the site using remotely sensed data. The square kilometer of leaf area index values 130 surrounding the tower site is shown in Fig. S5. A mean value of 0.8 was estimated using the landscape surrounding the site. The sensitivity to LAI can also be found in section 5 of the supplementary information. Additional information about each of Formatted: Subscript

Formatted: Subscript

Formatted: Subscript

Formatted: Subscript

the reported NEON datasets can be found in the Site Management and Event Reporting documentation (available at: https://doi.org/10.48443/9p2t-hj77).

NEON meteorological data contained gaps due to power outages and scheduled instrument maintenance. Across the year of data, the gaps comprised 5.8% of the data (1021 data points). To quantify the annual deposition of NH₃ in RMNP, these gaps were filled using the average diel pattern of fluxes during the current biweekly NH₃ sampling period.

2.2.2 Reanalysis meteorology data Meteorology Data

Detailed meteorological and soil data are not available at many locations where NH3 dry deposition is of interest. Reanalysis data, which combine short-range weather forecasts with assimilated observations, are a common source of meteorological data that can be used in the absence of local observations. To probe the impact of using reanalysis data in place of in situ observations, a set of bidirectional flux simulations was conducted using ERA5 hourly reanalysis data (Hersbach et al., 2020). ERA5 hourly reanalysis data has a spatial resolution of 0.25°, or approximately 31 km. The parameters used from the ERA5 data are as follows: air temperature, air pressure, dewpoint temperature, turbulent surface stress, moisture flux, sensible heat flux, friction velocity, standard deviation of filtered subgrid orography, solar radiation, and soil temperature. Obukhov length (L) is not given in the ERA5 dataset and was calculated using Eq. (1) following equation 5.7 from Stull (1988), shown below. Obukhov Length is the characteristic length scale of the atmosphere and is calculated from ERA5 data using instantaneous surface sensible heat and moisture fluxes based on the suggested calculation from the European Centre for Medium-Range Weather Forecasts (Gusti, 2024).

$$L = \frac{-\overline{\theta_v'} u_*^3}{k g \left(w' \theta_v'\right)_S} \frac{1}{L} = \frac{k g \left(tvst\right)}{T_{\frac{1}{2}} u_*^2},$$

(1)

135

140

150

160

where Where k is the von Karman constant, g is gravitational acceleration, $\overline{\theta_n}$ tyst is the mean turbulent temperature scale, T_v is the virtual temperature near the surface, $\overline{w' \theta_n}$ is the surface flux of virtual potential temperature, and u is the friction velocity.

2.3 NH₃ data Data

2.3.1 Biweekly NH₃ measurements Measurements

Biweekly NH₃ ambient air concentration was measured using Radiello (https://radiello.com/) passive diffusion samplers purchased from Sigma Aldrich... The Radiello sampling system includes a diffusive body (part number: RAD1201) and adsorbing cartridge (part number: RAD168), which is coated with phosphoric acid. NH₃ (g) diffuses across the exterior diffusive body and is collected on the adsorbing cartridge as ammonium (NH₄⁺) over two weeks. Collected ammonia (as NH₄⁺) is extracted from the cartridge into deionized water and analyzed on a cation IC using a 20 mM methanesulfonic acid eluent (0.5 mL min-1) on a Dionex CS12Ausing ion exchange column with a CSRS ULTRA II suppressor and Dionex conductivity

Formatted: Superscript

detectorehromatography (IC) (Li et al., 2016). NH₃ passive samples were collected in duplicate ($\sigma = \pm 0.25 \,\mu g \,m_k^{-3}$) on top of the NEON tower (25.35 m-agl). Across the study period, there were 27 sampling periods. In the case of overlapping sampling periods, a weighted average was calculated for each 2-week period. During the sampling period, some sampling periods were longer than others due to issues accessing the site. To compare periods of a consistent length, all data was taken to a 2-week average using a weighted mean of the data available during that period. One sample was below the detection limit and removed from this analysis. Passive NH₃ sampling methods have been shown to have a low bias when compared with other sampling methods, including annular denuders University Research Glassware Denuders and Picarro Cavity Ringdown spectroscopy methods (Pan et al., 2020; Puchalski et al., 2011).

170 2.3.2 High temporal resolution Temporal Resolution NH₃ measurements Measurements

NH₃ (g) air concentration was also measured using an ion mobility spectrometer (IMS). Ion mobility spectroscopy separates ionized molecules based on their mobility through a carrier gas, under the influence of an electric field. The instrument used was the AirSentry II Point-of-Use IMS (from Particle Measuring Systems, Niwot (Boulder, CO). The instrument was in the National Park Service (NPS) shelter (located at 40.278129, -105.545635) 500 meters north of the NEON site with an inlet located approximately 2 m above natural grassland. The sampling inlet was 0.635 cm 42 Teflon tubing, heated to 40 °C to reduce NH₃ loss to the sampling tube. Inlet length was kept as short as possible to further prevent NH₃ loss. Particles were removed by a fiber filter at the tip of the inlet. Due to the high altitude of the site location, the instrument was zeroed to account for pressure differences upon installation. Multi-point calibrations were conducted at the beginning and end of sampling. Calibration was confirmed using a known concentration ammonia gas sample split between the instrument and a phosphoric acid-coated denuder where the NH3 collected by the denuder is extracted into deionized water and analyzed using ion chromatography. Zero measurements were made periodically by overflowing the inlet with ultra-high purity clean air. The AirSentry samples at a 30-second frequency. During the study the AirSentry collected 919,000 data points. The limit of detection for 30-second measurements 70 pptv. For this data analysis, NH3 concentration data was averaged to 30-minute mean values. Averaging data points increases the signal-to-noise ratio. We approximate that the signal-to-noise ratio increases proportionally to the square root of the number of samples (n = 60) (Dempster, 2001). In this case, the signal-to-noise ratio increases by a factor of 7.7, reducing the limit of detection to 9 pptv for 30-minute mean NH₃ concentrations. Across the year of data collection, 101 points fell below the detection limit.

2.3.3 NH₃ data preparation Data Preparation

To investigate the effect of NH₃ (g) sampling time_-resolution<u>on simulated fluxes</u>, bidirectional fluxes were simulated with concentration data at: (i) 30-minute <u>resolutionfrequency</u> (30-minute NH₃), (ii) with the 2-week integrated passive NH₃ (Biweekly Passive NH₃), and lastly with an average diel profile applied to each day within the 2-week passive period (Average Diel Pattern NH₃). The three NH₃ data products are shown in Fig. 2.

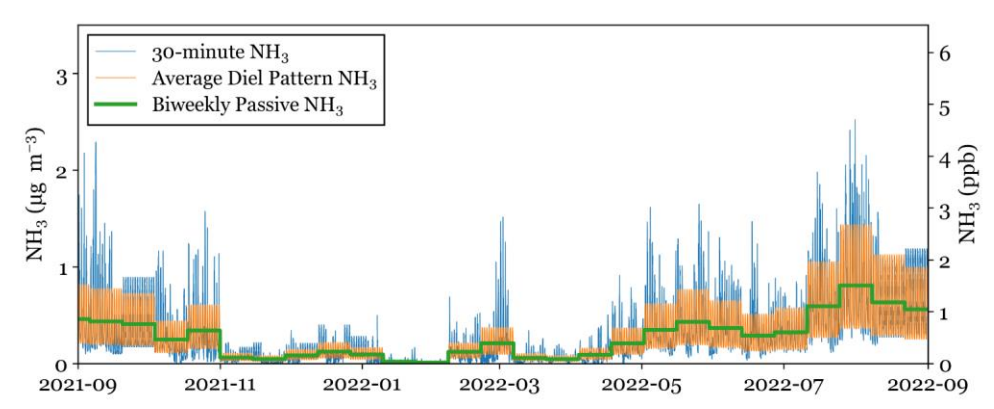


Figure 2. Three NH₃ concentration data sets are shown for the entire study period. The biweekly passive NH₃ is the mean of the NEON tower top duplicate measurements. 30 minute NH₃ data was generated using the AirSentry NH₃-concentration scaled to match biweekly passive NH₃ for each passive sampling period. Biweekly NH₃ with diel profile applied was generated by applying an average diel profile from the AirSentry NH₃ to each day of the biweekly passive measurement. The two-week average across each concentration data product is the same.

200

205

The 30-minute NH₃ concentration data is generated using a combination of data from the AirSentry NH₃ located at the NPS shelter and passive NH₃ samples collected on the NEON tower. Data gaps, due to power outages and regular maintenance, were filled using the average diel pattern across the year of data collection. Data gaps accounted for about 3000 out5-8% of more than 900,000 points the total data across the study period. To generate a 30-minute NH₃ data set above the tree canopy, the data was divided into biweekly periods that which match the passive NH₃ collection periods. The average concentration from the AirSentry across each period was then scaled to match the biweekly passive NH₃ concentration. The 101 NH₃ concentration values below the AirSentry detection limit, representing 0.5% of the total measurement period, were assumed to represent a random distribution below the detection limit and retained for post-process scaling from the passive observations. This preserves the temporal variability of NH₃ concentrations while ensuring that the average air concentration across the sampling period is consistent with the passive NH₃ measurements atop the NEON tower, which can differ from those above the adjacent grassland where the Air Sentry measurements are made.

210 The biweekly passive NH₃ with diel profile applied is generated using the annual average diel pattern of NH₃ from the AirSentry data. To determine if there are systematic differences between the NH₃ diel pattern at the two sites, raw and scaled AirSentry concentrations were compared to 4- and 6-hour University Research Glassware denuder measurements taken on the NEON tower. The NH₃ concentrations were well correlated between sites. This comparison is shown in Fig. S1. Each day of the biweekly passive period is assigned the average diel pattern, then the biweekly mean is scaled to match the biweekly passive concentration. This dataset was generated to investigate if the inclusion of a simple diel profile was sufficient to correct for the bias in bidirectional fluxes created by using low time-resolution NH₃ concentrations as shown by Schrader et al. (2018).

These three concentration data sets will be used for bidirectional flux simulations of NH₃. For the rest of this work, the three NH₃ data sets will be referred to using the following nomenclature.

30-minute NH₃: NH₃ concentration data at 30-minute resolution frequency

Biweekly NH3: Biweekly Passive NH3 concentration data

Average Diel Pattern NH₃: Passive NH₃ concentration scaled using an average diel profile from the 30-minute NH₃ dataset

2.4 Additional measurements Measurements

2.4.1 Wet deposition data Deposition Data

220

Weekly precipitation wetWet deposition data was obtained from the National Trends Network (NTN) (National Atmospheric Deposition Program, 2022) site at Beaver Meadows in RMNP ('CO19': located at 40.36393639*N, -105.58105810*E). The Beaver Meadows site location, at 2477 m elevation and located approximately 10 km north of the CASTNET site, is shown in Fig. 1.

2.4.2 Additional gasGas and particle measurements Particle Measurements

Additional air concentration data was obtained from the U.S. EPA Clean Air Status and Trends Network (CASTNET) site at the NPS shelter ('ROM206': located at 40.278129, -105.545635). Weekly filter pack concentrations of nitric acid (HNO₃) and sulfur dioxide (SO₂) were used to calculate the acid ratio (Eq. 10equation 8) in the bidirectional exchange simulations of NH₃ (U.S. EPA, 2024a).

Weekly dry deposition of HNO₃, NO₃, and NH₄⁺ was <u>estimatedgenerated</u> by CASTNET (US EPA, 2024b) using the weekly filter pack concentrations and historical values of deposition velocity (V_d) from the U.S. EPA Multi-Layer Model (MLM) (Meyers et al., 1998). The generation of deposition velocities was discontinued in 2019. Bowker et al. (2011) found that using historical values of <u>V_afromdeposition velocity from</u> the U.S. EPA Multi-Layer Model did not significantly bias the annual mean of deposition.

One approach to estimating NH_3 deposition is to estimate the deposition velocity (V_d) as a fixed fraction (70%) of the $\underline{V_{dof}}$ deposition velocity of HNO₃. This approach has been historically used to estimate the $\underline{V_{dof}}$ deposition velocity of NH_3 in RMNP (Beem et al., 2010; Benedict et al., 2013a; Benedict et al., 2013b).

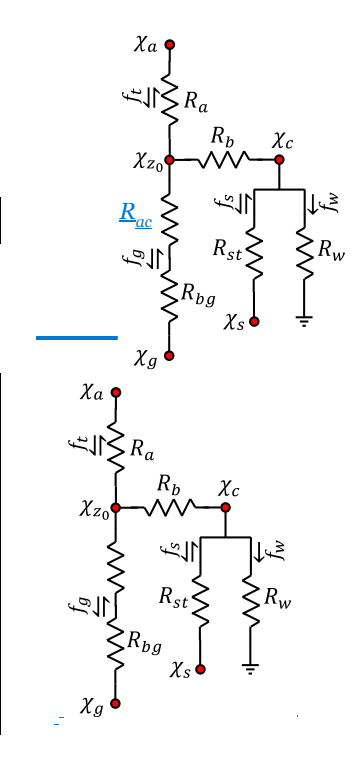
$$V_d(NH_3) = 0.7 * V_d(HNO_3),$$
 (2)

2.5 Bidirectional $\underline{flux\ modelling}Flux\ Modeling}$ of NH_3

Bidirectional NH₃ fluxes are simulated across the study period using the dry deposition inferential model described in Massad et al. (2010). This model was selected because it estimates both emissions and deposition of NH₂, uses a compensation point framework to capture these complex dynamics, and takes into account rapidly changing micrometeorology. The simulation

Formatted: Subscript

framework (Fig. 3) accounts for the bidirectional nature of NH₃ fluxes and allows for deposition and emission. The model determines if the flux will be negative (deposition) or positive (emission) based on the relationship between the atmospheric concentration (χ_a) at a given reference height (z) and the eanopy compensation point (χ_{a0}) at a defined distance (d) above χ_a). Canopy compensation point depends on the roughness length (z_0), stomata resistance, cuticle resistance, and stomata compensation point.



250

χа	Atmospheric ammonia concentrationConcentration	χс	Canopy compensation point
χz0	Reference Height (Z_0) Compensation point at $(d + z_0)$	χg	Ground layerSoil compensation point
R_a	Aerodynamic resistance	$\chi_{\rm s}$	Stomata compensation point
R_b	Laminar boundary layer resistance	f_t	Total <u>flux</u> Flux

Formatted Table

	R_{bg}	Ground laminar boundary layer	f_g	Ground <u>flux</u> Flux
		resistance		
255	$R_{\rm w}$	<u>Cuticular</u> Cuticle resistance	f_s	Stomatal fluxStomata Flux
	R_{st}	Stomatal Stomata resistance	$f_{\rm w}$	Cuticular flux Cuticle Flux
	Rac	Aerodynamic resistance in the canopy		

260

275

Figure 3. Dry deposition inferential model proposed in Massad et al. (2010). The table describes each model element. Arrows next to each flux show the allowed flux directions of the given pathway.

A conceptual diagram of resistances and compensation points is shown in Fig. 3. Aerodynamic (R_a) and laminar boundary layer resistance (R_b) capture the effects of turbulent and diffusive transfer from the atmosphere to the surface, respectively. R_a was calculated according to Thom (1975), where z is reference height (25.35 m_a), d is the displacement height (7.15 m_a), and z_0 is the roughness length is height (1.65 m_a). The stability functions are Ψ_H and Ψ_M for scalars and momentum, respectively, are empirical relationships dependent on L (Thom 1975). Displacement and roughness lengthheights were provided from the RMNP NEON Tower (NEON, 2023).

$$R_a = (k \bullet u^*)^{-1} \bullet \left(\ln \left(\frac{z-d}{z_0} \right) - \Psi_H + \Psi_M \right), \tag{3}$$

270 R_b is modeled as described in Xiu and Pleim (2001), where γ_{air} is the kinematic diffusivity of air, and D_{NH3} is the diffusivity of NH₃.

In-canopy aerodynamic resistance (R_g) is R_{isc} captures the sum of aerodynamic resistance from within the canopy (R_{ac}) and ground boundary layer resistance (R_{bg}) . R_{ac} and was calculated based on Nemitz et al. (2001) using Eq. (5) where α is a height dependent constant calculated using Eq. 16 and Eq. 17 from equations 15–17 of Massad et al. (2010).

$$R_{ac(d+z0)} = \frac{a_{(d+z0)}}{u^*} \tag{5}$$

(2010). Ground boundary layer resistance (R_{bg}) is based on Nemitz et al. (2001), where $\underline{u}_{g}\underline{u}$ is the wind speed at the ground, which we approximate as 5% of the wind speed at tower top (25eanopy height (h=11 m), and z_{i} is the upper bound height of the logarithmic wind profile above the ground, which we approximate as 10% of the canopy height (Nemitz et al., 2001) R_{bg} =

$$\begin{pmatrix} \frac{\gamma_{air}}{D_{NH_3}} - \ln\left(\frac{D_{NH_3}}{k * u_g * z_I}\right)\right) \bullet \frac{1}{k * u_g}, \tag{6}$$

$$R_{\underline{Bg}} = \begin{pmatrix} \frac{\gamma_{air}}{D_{NH_3}} - \ln\left(\frac{D_{NH_3}}{k * \frac{u_g}{2a} \cdot 0.1 * k}\right)\right) \bullet \frac{1}{k * \frac{w}{2a}}, \tag{5}$$

Stomata resistance (R_{st}) captures the diffusion of NH_3 through plant stomata and is calculated as a minimum value related to the plant type proposed by Hicks et al. (1987). Further parameterization proposed by Nemitz et al. (2001) was used here to calculate R_{st} , where SR (W W⁻²) is the solar radiation. The minimum value for R_{st} (225 s W⁻¹) was determined using Table 1 of

Zhang et al. (2003), assuming 75% of the land surface was evergreen needleaf trees and 25% was deciduous broadleaf trees and shrubs.(2003).

$$R_{st} = \min\left\{5000 \ (s \ m^{-1}), 225 \ (s \ m^{-1}) \bullet \left(1 + \left(\frac{180}{sR}\right)\right)\right\},\tag{76}$$

<u>CuticularCuticle</u> resistance (R_w) was calculated according to the proposed <u>corrected parameterizationas</u> <u>described parameterization</u>, for forest ecosystems of predominantly <u>Douglas Fir</u>, in Massad et al. (2010), for a forest ecosystem.). When relative humidity (RH) is below 100%, <u>Eq. (8) equation 7</u> is used and when RH exceeds or is equal to 100%, <u>Eq. (9) equation 8</u> is used.

$$R_w = 31.5 \cdot \frac{1}{AB} \cdot e^{(0.0318(100 - RH))},$$
 (87)

$$R_{W} = \frac{31.5}{4R},\tag{98}$$

In both equations, AR is the acid ratio which is calculated using the molar ratio of acids and bases in the atmosphere. The calculated acid ratio had a mean value of 1.3, a minimum of 0.22, and a maximum of 11.6. Acid ratios were the largest in the winter months.

$$AR = \frac{2 \cdot [SO_2] + [HNO_3]}{[NH_3]}, \tag{109}$$

For this study period, the acid ratio was calculated using weekly CASTNET measurements of SO₂ and HNO₃ paired with our measurements of NH₃.

300 χ_{st} wasStomata compensation points were calculated according to Massad et al. (2010). In the stomata compensation point (Eq. 11 equation 10), Γ_{st} is the emission potential of the stomata and is approximated as 294 based on vegetation samples from the area surrounding the NEON Tower. The sampling methods and determination of this value can be found in the supplementary information. Emission potentials describe the potential for surface emission. Massad et al. (2010).

$$\chi_{st} = \frac{2.7457 \cdot 10^{15}}{T} \cdot e^{\left(-\frac{10378}{T}\right)} \cdot \Gamma_{st} , \qquad (\underline{1140})$$

305 X_ewas Soil compensation point was calculated according to Eq. (equations 3) through Eq. (5) of Stratton et al. (2018). In Eq. (12)_{equation 11}, TAN is the concentration of total ammoniacal ammoniacal N (the sum of NH₃ and NH₄⁺) in the soil aqueous phase (mg kg⁻¹), K_H is the Henry constant, and K_a is the equilibrium constant. TAN was estimated at 109.6 mg kg⁻¹ based on soil measurements in RMNP from Stratton et al. (2018). NH₃ flux simulations are very sensitive to TAN value. The supplementary information includes a test of the sensitivity of the flux results to TAN values within one standard deviation for

310 the measurements taken by Stratton et al. (2018).-

$$\chi_g = \frac{\kappa_H}{1 + (10^{-pH})/(\kappa_0)} \bullet TAN$$
, (12++)

 K_H and K_a were predicted using Eq. (13) equations 12 and Eq. (14)13 based on the models of Montes et al. (2009), where T is temperature.

$$K_H = \left(\frac{0.2138}{T}\right) \cdot 10^{(6.123 - 1825/T)}$$
, (1342)

315
$$K_a = 10^{\left(0.05 - \frac{2788}{T}\right)},$$
 $\left(\frac{1413}{T}\right)$

Commented [LN1]: Add the citation to the paper from Jay Hamm's group

χ_c, Eq. (15) Canopy compensation point (equation 14 below₃) was calculated using Eq. (equation-12) from Massad et al. (2010).

$$\chi_{c} = \frac{\chi_{a} * (R_{a} * R_{b})^{-1} + \chi_{s} t^{*} [(R_{a} * R_{s}t)^{-1} + (R_{b} * R_{s}t)^{-1} + (R_{g} * R_{s}t)^{-1}] + \chi_{g} * (R_{b} * R_{g})^{-1}}{(R_{a} * R_{b})^{-1} + (R_{a} * R_{w})^{-1} + (R_{b} * R_{g})^{-1} + (R_{b} * R_{s}t)^{-1} + (R_{g} * R_{w})^{-1} + (R_{g} * R_{w})^{-1}} + (R_{g} * R_{w})^{-1} +$$

320 Compensation point at the <u>a displacementreference</u> height (<u>d</u>) above the roughness length (<u>z</u>₀)Z₀ is calculated using Eq. (16) equation 15 below as proposed in Massad et al. (2010). χ₂₀The reference height is the same as the height at which NH₂ measurements were taken. The reference height compensation point takes all other compensation points and resistances into account.

$$\chi_{20} = \frac{\left(\frac{\chi_{a_1} + \frac{\chi_{g}}{R_g} + \frac{\chi_{c}}{R_b}}{\left(\frac{1}{R_b} + \frac{1}{R_b} + \frac{1}{R_b}\right)}}{\left(\frac{1}{R_b} + \frac{1}{R_b} + \frac{1}{R_b}\right)},\tag{1645}$$

325 Finally, the total flux was calculated following Eq. (17 equation (16) (Massad et al., 2010). NH₃ flux is calculated defined in this framework as a difference between the χ_{zo} and χ_a reference height compensation point and the NH₃ concentration at that height, scaled by R_athe aerodynamic resistance.

$$F_{NH_3} = \frac{\frac{\chi_{20} - \chi_a}{R_a}}{(17\frac{\chi_{20} - [NH_3]}{R_{12} + 10^2}},$$

330 (16)

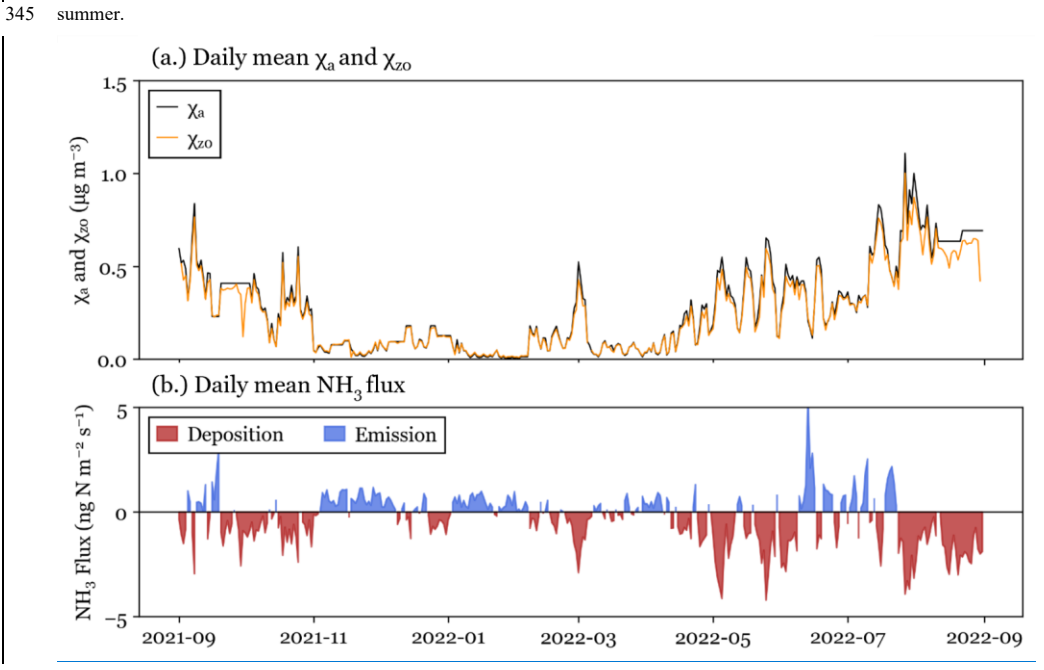
Total exchange flux (F_{NH3}) from the dry deposition inferential model gives the direction and magnitude of NH₃ fluxes.

3. Results and Discussion

3.1 Simulated bidirectional exchange fluxes Bidirectional Exchange of NH₃

Bidirectional fluxes were simulated using the 30-minute NH₃ concentration data set and in situ meteorological data as inputs to the Massad et al. (2010) model, described above. NH₃ concentration, χ₂₀ reference height compensation point, and fluxes have a strong seasonal cycle in RMNP (see Fig. 4). NH₃ flux direction is determined by the difference between χ₂₀ relative magnitudes of the NH₃ concentration and χ₄the reference height compensation point, (Fig. 4a.). When NH₃ concentration exceeds the compensation point, NH₃ is deposited to the surface (a negative flux value). Both NH₃ concentrations and deposition fluxes tend to be greatest during the summer (June, July, and August), with 4748% of NH₃ modeled annual dry deposition occurring during June, July, and August. NH₃ fluxes also had the largest variability in the summer. Deposition in the spring (March, April, and May) closely follows, with 4333% of NH₃ modeled annual dry deposition occurring during March, April, and May. During all seasons there are periods of net emission from the surface (Fig. 4b.). The largest periods of net emission occur in the summer. DailyThese daily NH₃ emission fluxes are most common in the winter (December, January,

Formatted: Font color: Dark Red
Formatted: Font color: Dark Red



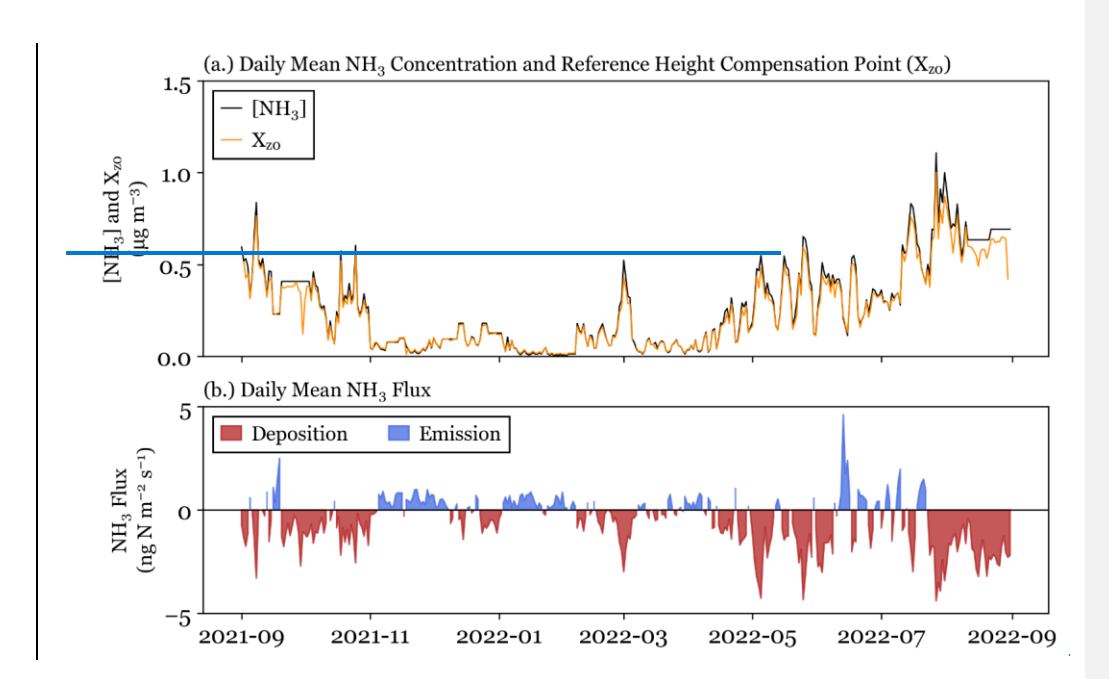


Figure 4. Daily mean values of: (a.) Daily mean χ_a NH₃-concentration and χ_{a0} reference height compensation point, and (b.) NH₃ flux.

Total modeled NH₃ flux can be broken down into stomatal stomata, ground, and cuticular entire fluxes. Figure 5 shows the

distribution of simulated NH3 fluxes for each of these components.

Deposition is driven primarily by <u>stomatalstomata</u> and <u>cuticulareutiele</u> fluxes, while ground emission fluxes are sometimes observed. Winter periods of net emission (see Fig. 4b.) are driven by the ground flux. One potential limitation of the model used for simulations is that it does not consider snow cover on the ground, which could alter winter fluxes in RMNP.

Formatted: Font color: Dark Red, Subscript

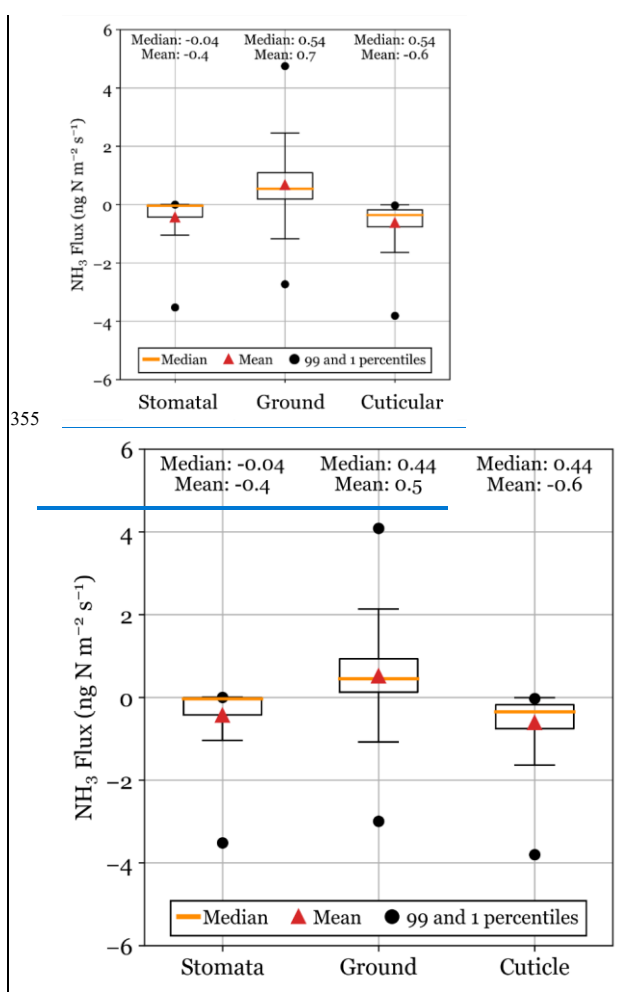


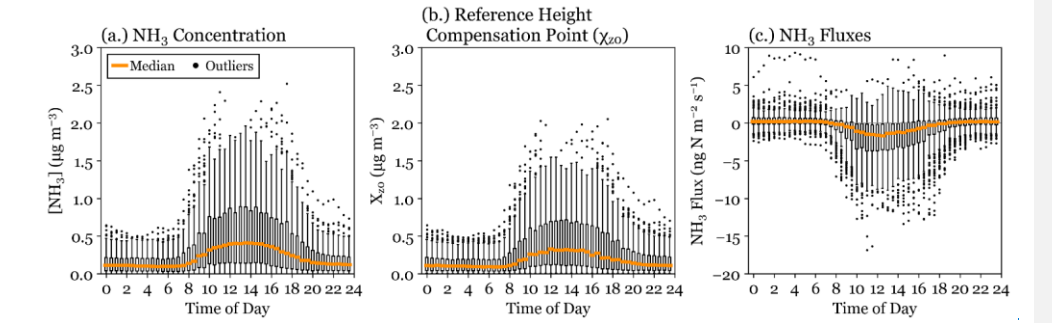
Figure 5. Total NH₃ simulated fluxes are separated into their component fluxes (<u>stomatalstomata</u>, ground, and <u>cuticulareutiele</u>). Simulated fluxes are shown for the entire study period. Boxes show the 25th and 75th percentile, and whiskers are determined at 1.5 times the interquartile range.

360 NH₃ concentrations at RMNP are impacted by emission and transport patterns, which can both increase daytime NH₃ concentrations. NH₃ emissions from agricultural sources have a strong diel pattern driven by volatilization during warmer

daytime temperatures. At RMNP, transport from these regions is driven on many days by the mountain-plains circulation, which begins in the late morning and transports polluted air masses westward and upslope to the park (Gebhart et al., 2011). Previous studies have demonstrated that the upslope transport from sources in the Front Range has impacts on deposition and air concentrations in RMNP (Benedict et al., 2018; Pan et al., 2021). During this study, the largest χ_θ values are also observed during upslope transport from source regions in the CO Front Range. These source regions likely disproportionately contribute to NH₃ dry deposition because the difference between χ_θ and χ_θ drives the sign and magnitude of the NH₃ flux. On mornings following overnight dew formation, local volatilization from evaporating dew has also been shown to increase morning NH₃ concentrations (Wentworth et al., 2016). This phenomenon was observed in RMNP and corresponds to the increase in the NH₃ diel pattern around 10:00 observed in Fig. 6a. One limitation of the bidirectional flux model used is that NH₃ uptake and emission from dew are not simulated. NH₃ concentration, compensation point, and simulated fluxes each have a strong diel pattern, which peaks during the middle of the day (see Fig. 6). The peak value typically occurs close to 13:00. The soil temperature diel pattern contributes to a higher χ_ω reference height compensation points during the middle of the day. The annual cycle of soil temperature also contributes to the higher χ_ω reference height compensation points observed in summer. Although both NH₃ concentration and compensation point peak during the mid-day, we also observe peak deposition fluxes during the middle of the day, indicating that the influence of the diel pattern of NH₃ concentration is stronger than that from

370

the compensation point diel pattern.



Formatted: Subscript

Formatted: Subscript

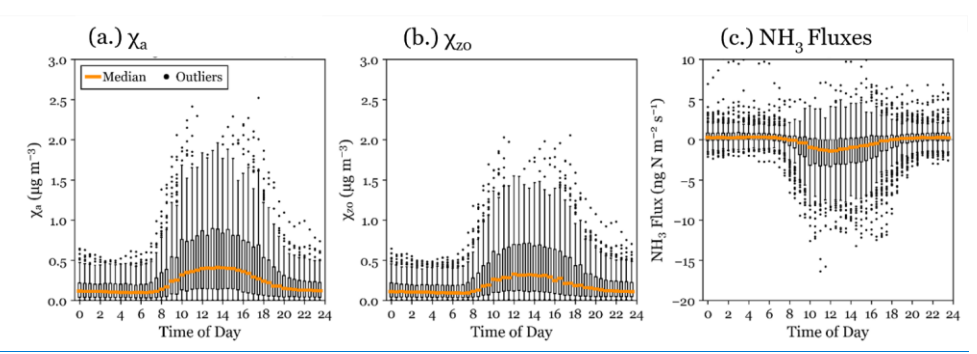
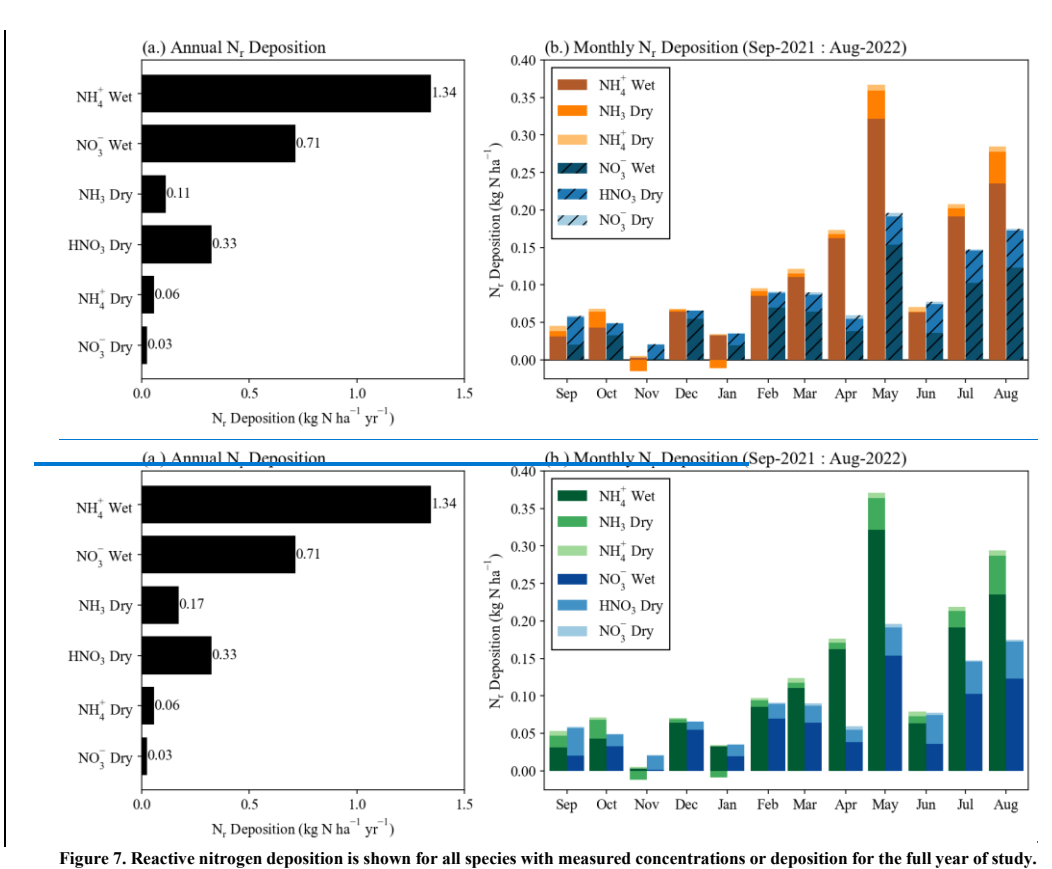


Figure 6. Diel pattern of: (a.) NH3 concentration, (b.) simulated <u>yea reference height compensation point</u>, and (c.) NH3 fluxes are shown for the full study period in RMNP. Boxes show the 25th and 75th <u>percentilespercentile</u>, and whiskers are determined at 1.5 times the interquartile range.

385

To understand the relative importance of NH₃ deposition in RMNP, NH₃ flux simulation results are combined with NADP/NTN wet deposition fluxes and dry deposition fluxes for particulate ammonium (NH₄⁺) and nitrate (NO₃⁻) and gaseous HNO₃ derived from CASTNET concentration observations and MLM deposition velocities, to construct an updated seasonal and annual budget of inorganic N deposition at RMNP. This N_r deposition budget for all measured inorganic species is shown in Fig. 7a. Due to the lack of current measurements, wet and dry deposition of organic nitrogen are not included. Benedict et al. (2013b) reported annual organic nitrogen wet deposition of 0.6 kg N ha⁻¹ yr⁻¹ during their 2008-2009 study. NH₃ dry deposition is the net surface flux from the simulations using 30-minute NH₃ concentration. The inorganic annual N_r deposition budget totals 3.4 kg N ha⁻¹ yr⁻¹, with the largest contributions coming from NH₄⁺ wet deposition (1.34 kg N ha⁻¹ yr⁻¹), NH₃ net dry deposition (0.1247 kg N ha⁻¹ yr⁻¹), NO₃⁻ wet deposition (0.71 kg N ha⁻¹ yr⁻¹), and HNO₃ dry deposition (0.33 kg N ha⁻¹ yr⁻¹). Overall, reduced N_r deposition comprises 5960% of the total inorganic N deposition to RMNP. NH₃ dry deposition comprises 46% of total inorganic N_r deposition. Simulated NH₃ dry deposition (0.1147 kg N ha⁻¹ yr⁻¹) is smaller than the value estimated by as the NH₃ concentration multiplied by 0.7 times the HNO₃ deposition velocity by Scaling the HNO₃ dry deposition velocity by scaling the HNO₃ dry deposition velocity by 1.7, instead of simulating the bidirectional exchange of NH₃.



400 Wet deposition data is from the NADP NTN site at Beaver Meadows. NH₃ deposition is modeled using the bidirectional framework from Massad et. al (2010) and 30-minute NH₃ concentration data. Dry deposition of HNO₃ (g), NH₄⁺ (p), and NO₃ (p) are calculated from the nearby CASTNET site concentration data and deposition velocities from the U.S. EPA MLM. Panel (a.) has the annual deposition of all measured species. Panel (b.) has deposition of all measured N₇ species grouped by month. Reduced-N species are green. Oxidized N species are blue. Only one period of wet deposition was collected by the NADP NTN site during 405 November 2021.

Speciated monthly dry deposition is plotted in Fig. 7b to probe the seasonality of N_r deposition in RMNP. Net dry deposition of NH₃ was largest during May-July and August. Total inorganic N_r deposition peaked during May, due to increased wet deposition. Reduced For all months except November and January, reduced N_r deposition exceeded oxidized N_r deposition in October, December, February, March, April, May, July, and August. Excluding November, where only one period of wet

deposition was recorded by the NADP NTN site, reduced N_r deposition had, with a fractional contribution ranging from 4347 to 7475%. In November and January, net NH₃ emission was estimated from the surface.

3.2 Impacts of biweekly Biweekly NH₃ concentration data Concentration Data on simulated fluxes Simulated Fluxes

The use of low time-resolution NH3 concentrations for flux simulations can produce a low bias compared with fluxes simulated using higher time-resolution NH₃ concentrations. Simulated NH₃ fluxes have Here, we follow a strong diel pattern when simulated at 30-minute resolution (see Fig. 6c), due similar method to changes in NH₃ concentration and meteorology. These complex dynamics are averaged out when an average NH3 concentration is used, which leads to an underestimation in deposition. Here, wethat described by Schrader et al. (2018) and demonstrate that a site-specific correction can be generated to account for the bias introduced by lower time-resolution NH3 concentration data. Our methods differ from Schrader et al. 420 (2018) in 3 major ways: (i) in situ data is used for both the higher frequency, 30-minute NH₃ concentration, and meteorology, (ii) biweekly passive NH3 data is used instead of monthly NH3 data, and (iii) Massad et al. (2010) is used as described instead of using a simplified parameterization. The results of the 30-minute NH₃ and Biweekly NH₃ bidirectional NH₃ flux simulations are compared to generate a site-specific factor to correct for any low bias in the lower time--resolution flux calculations. Simulated fluxes at biweekly time-resolution (Fig. 8) using the two NH₃ concentration data sets are well correlated (R^2 0.88),89) and the NH₃ flux simulation using biweekly integrated NH₃ data can be corrected to match the control flux simulation using a linear fit (slope: 1.0307, y-intercept: -1.689468). As noted above, RMNP has few two-week periods of net NH₃ emission, and the efficacy of this method should be confirmed at a location with more extensive periods of net NH₃ emission. In particular, NH3 fluxes above managed agricultural land could differ significantly from the pattern observed in RMNP. This study also focused on fluxes above a forest canopy, and results could differ for grassland ecosystems, which also occur in RMNP. To determine the efficacy in other locations, future investigations should select several sites with different land surface types and NH₃ concentrations to make biweekly and high_time_resolution measurements for a year.

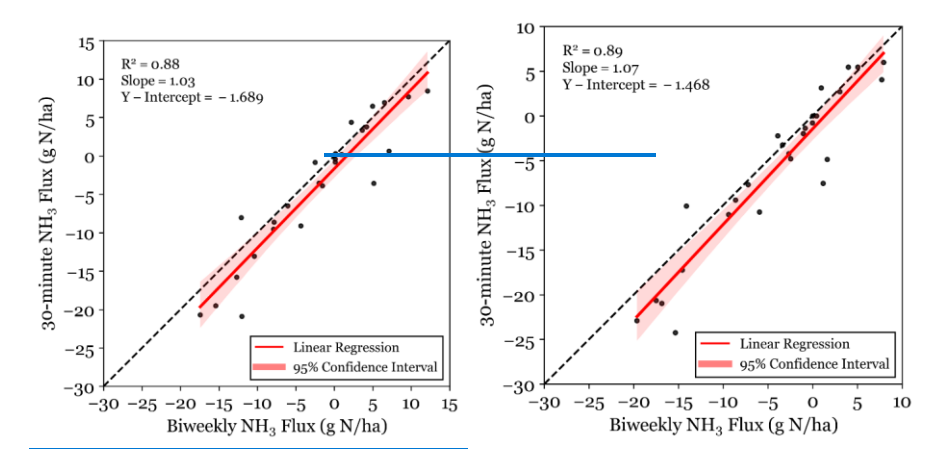
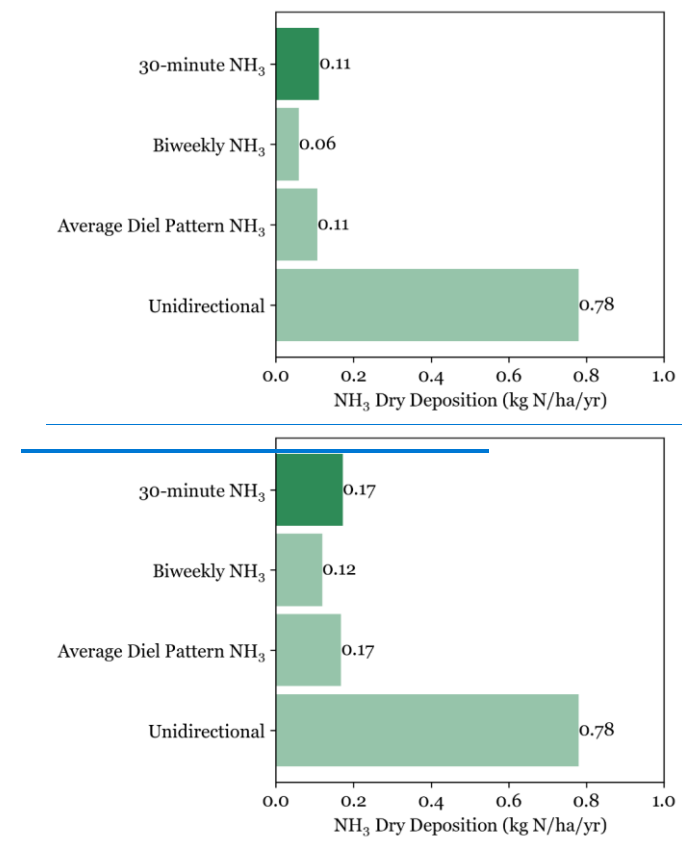


Figure 8. Bidirectional NH₃ flux simulated at 30-minute resolution is plotted for 30-minute NH₃ concentration data and biweekly integrated NH₃ concentration data. Fluxes are given as net flux over a two-week period. The least squares linear regression is plotted for the data.

Considering the net flux of NH₃ across the full study period, using the best available time_resolution of 30 minutes, we find a total annual net NH₃ dry deposition flux of $0.\underline{1147}$ kg N ha⁻¹ yr⁻¹ (Fig. 9). The estimated NH₃ dry deposition drops by $\underline{45299}$ % to $0.\underline{0642}$ kg N ha⁻¹ yr⁻¹ using biweekly vs. 30-min NH₃ concentration measurements. The annual NH₃ dry deposition flux increases to 0.78 kg N ha⁻¹ yr⁻¹ when simulating fluxes in a deposition-only unidirectional framework where the NH₃ deposition velocity is scaled as 0.7 times the nitric acid deposition velocity (<u>estimatedgenerated</u> by the US EPA MLM), an approach previously used for RMNP N deposition budgets (Beem et al., 2010; Benedict et al., 2013a; Benedict et al., 2013b).

440



445 Figure 9. Annual NH₃ dry deposition at the NEON Flux Tower in RMNP is shown for three bidirectional simulations using three sets of NH₃ concentration data (30-minute NH₃, Biweekly NH₃, and Average Diel Pattern NH₃) and one unidirectional simulation. Each simulation was run at 30-minute time steps with meteorological parameters from the NEON Flux Tower. The unidirectional NH₃ flux is calculated using simulation uses biweekly NH₃ concentrations, NH₃ and deposition velocities are calculated as 0.7 times the HNO₃ deposition velocity from based-on the U.S. EPA MLM.

Bidirectional flux simulations using biweekly NH₃ data with an average diel pattern of NH₃ yield the same annual NH₃ dry deposition flux as the simulations run using 30-minute NH₃ concentration. This indicates that capturing daily variability in NH₃ concentration profiles is not critical to accurately simulating the annual NH₃ flux. Application of an annual averaged diel pattern misses the highest NH₃ concentrations (Fig. 10), however, across a full year of data the diel pattern effectively captures the net surface flux. Despite the scatter in Fig. 10a., fluxes simulated with an average diel pattern NH₃ data set are well

Formatted: Subscript

455 correlated with simulations using 30-minute NH₃ concentrations (R²=0.596) and have a fit close to unity. The daily mean fluxes (Fig. 10b and Fig. 10c) of each simulation have similar seasonal patterns, with periods of net emission and deposition aligned between simulations.

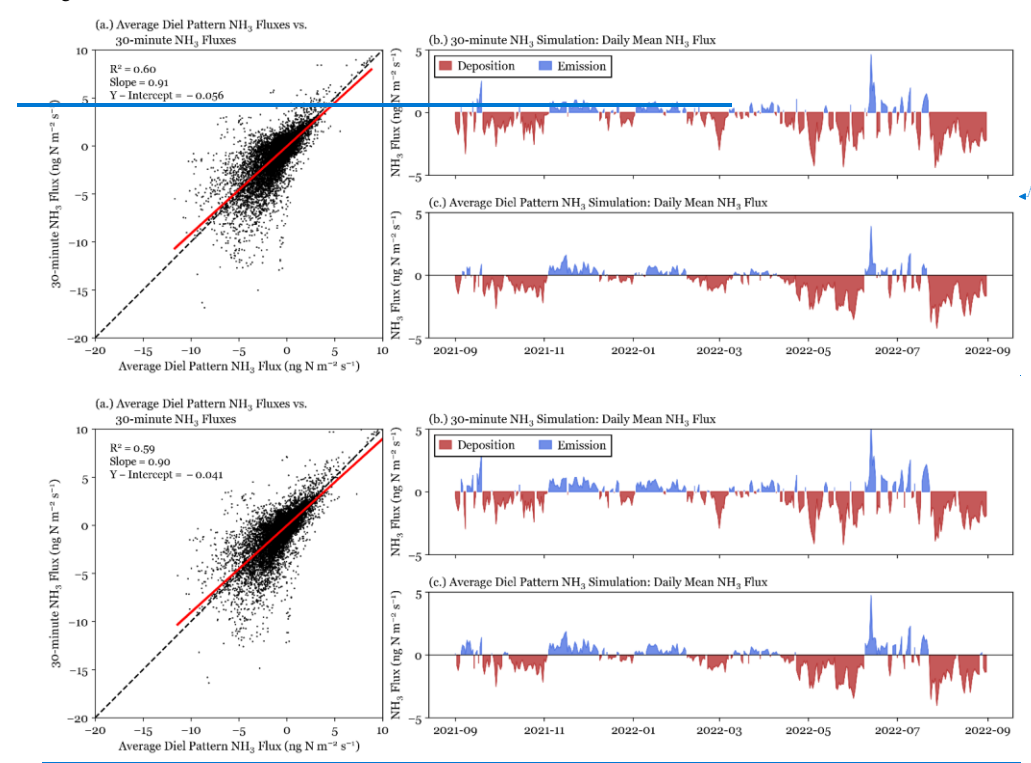


Figure 10. NH₃ fluxes simulated with 30-minute NH₃ concentrations and annual average diel pattern NH₃ concentrations are shown for the full year of data. Panel (a.) directly compares 30-minute simulated fluxes for each data set. Panels (b.) and (c.) show the daily mean fluxes for simulations with 30-minute NH₃ concentration and average diel pattern NH₃ concentration_a respectively.

At RMNP, there is a large daily variability in concentration due especially to changes in upslope transport. When an air mass arrives from the Colorado Front Range and NE Colorado, NH₃ concentrations rise significantly due to the large emission sources upwind. For the comparison shown in Fig. 10, the diel pattern was determined using a full year of NH₃ concentration data. Fluxes were also simulated using diel patterns determined with only a month of data, to probe the necessary length of measurements to generate an effective diel pattern. Annual deposition from all flux simulations using <u>each different a</u> monthly diel pattern fell within 2% of the annual deposition using the annual average diel pattern. Therefore, in RMNP, one month of

465

Formatted: Normal

30-minute measurements appears sufficient to generate a diel pattern that which will effectively correct the net NH₃ surface flux. Other locations may have larger and/or more complex variability in NH₃ diel pattern and may require longer periods of data collection to establish an NH₃ diel pattern.

470

480

485

3.3 Impacts of reanalysis meteorological dataReanalysis Meteorological Data on simulatedSimulated NH3 fluxes

Bidirectional exchangeDry deposition inferential models require several meteorological and soil parameters, which may not be readily available for many locations of interest. Reanalysis data can provide meteorological inputs for locations where required in situ meteorological and soil measurements are unavailable. To examine the impact on flux simulation accuracy resulting from this substitution at RMNP, the same simulations of NH₃ bidirectional fluxes were run using ERA5 meteorology and soil data. 30-minute NH₃ simulations run with reanalysis data inputs are well correlated ($R^2 = 0.7680$) with 30-minute NH₃ simulations run with in situ data inputs (see Fig. 11+1a) but overestimate the annual NH₃ deposition flux by a factor of 2.59%. From Fig. 11.41a., we find that the use of ERA5 reanalysis data in the simulation of NH₃ bidirectional fluxes introduces a low bias to the flux magnitude in RMNP compared to in situ meteorological data, for both positive (emission) and negative (deposition) fluxes. However, because the decrease to deposition fluxes is smaller than the decrease to emission fluxes, we observe an The annual overestimation from simulations using ERA5-is due in large part to missing periods of surface emission. Based on this result, ERA5-reanalysis data should not be used to estimate NH₃-fluxes before additional sites and data have been considered using in situ data.

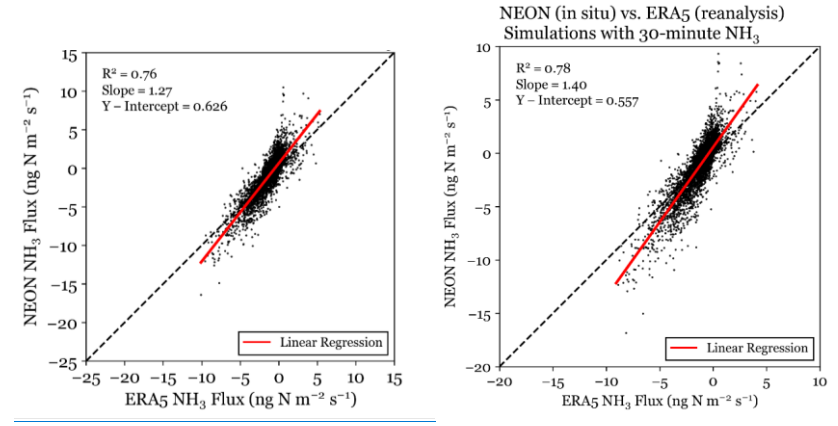
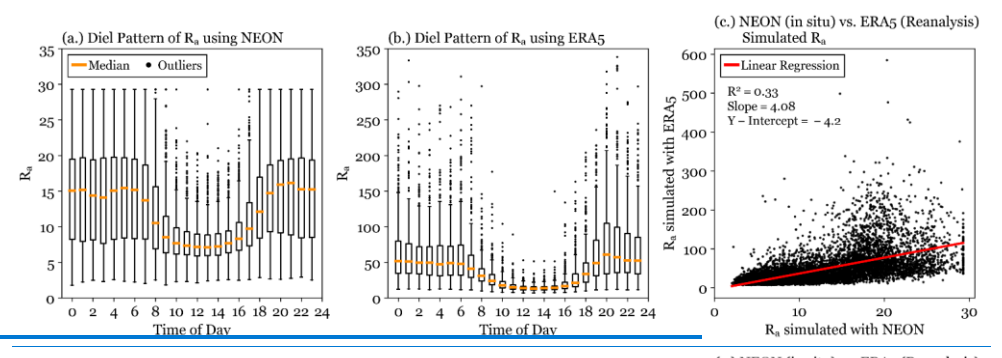


Figure 11. Bidirectional NH₃ flux simulated with ERA5 meteorology and NEON meteorology at 30-minute resolution using the 30-minute NH₃ concentration. The least squares linear regression is plotted for the data in red.

The low bias for fluxes simulated using ERA5 reanalysis data is investigated further to explore what parameterssparameter differences influence this bias. Net NH₃ fluxes are simulated using Eq. (17Equation (12), which relies on χ_{20} , NH₃

concentration, and aerodynamic resistance (R_{ac}). We find that the simulations using reanalysis data generate reference height compensation points (χ_{20}) which agree well with the simulations using that used in situ measurements ($\chi_{20} = 1.03$ Slope=0.94, $R^2 = -0.98$).



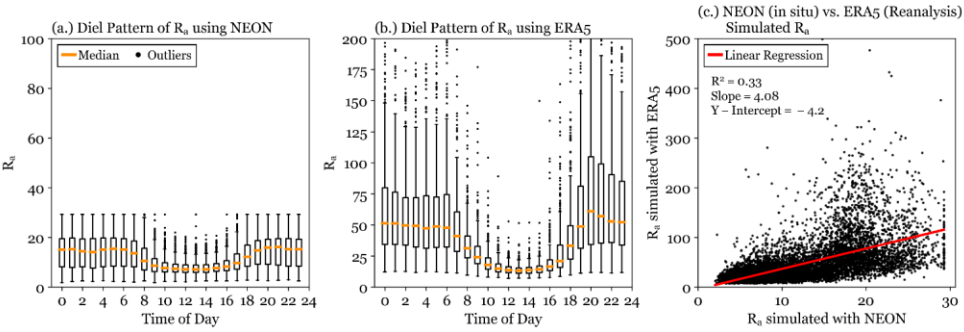


Figure 12. Aerodynamic resistances are shown for simulations using in situ meteorological data from the NEON flux tower and reanalysis meteorological data from ERA5. The diel patterns are shown in panels (a.) and (b.) respectively. Panel (c.) directly compares simulated Ra values using NEON in situ and ERA5 reanalysis data.

Although the general diel pattern of R_a is well captured using reanalysis data, R_a magnitudes differ substantially between the two simulations (Fig. 12a and 12b), with the largest difference occurring overnight.) Maximum R_a values from the reanalysis simulations are greater than an order of magnitude larger than those derived using in situ meteorology. A and a comparison of the two data sets shows (Fig. 12c) a typical enhancement of approximately a factor of four. Increased R_a values result in lower simulated NH₃ fluxes. The R_a bias is likely driven by differences in the friction velocity (u_2) and u_3 0 and u_4 0 and u_4 0 and u_4 0 are used to calculate simulate u_4 0. ERA5 data underestimates u_4 0 by a factor of 5 when compared with the in situ NEON data (u_4 0 and u_4 0

Formatted: Font: Italic

Formatted: Subscript

Formatted: Subscript

in modeled R_a may be due to the gridded nature of reanalysis data, which represents a large area of variable land types and complex topography using only a single value (Hogrefe et al., 2023). Obukhov Length is the characteristic length scale of the atmosphere and is calculated from ERA5 data using surface sensible heat and moisture fluxes. Previous work has identified heat and moisture fluxes as large areas of uncertainty in ERA5 Reanalysis (Kong et al., 2022; Mayer et al., 2022). Two case studies were conducted to probe the relative importance of u_e and L. The case studies are described in the supplementary information. Differences in R_a were impacted by both u_e and L, accounting for 23% and 10%, respectively, of the discrepancy between in situ and ERA5 flux simulations. Comparisons of all meteorological parameters used can be found in the Supplement.

4. Conclusion

510

535

Fluxes of NH₃ (g) can be are best simulated using a bidirectional model, which uses rapidly changing meteorology paired with air concentrations and soil parameters to infer flux direction and magnitude. We use a bidirectional NH₃ flux model, proposed by Massad et al. (2010), to simulate a year of NH₃ fluxes above a subalpine forest ecosystem in Rocky Mountain National Park. The net NH₃ dry deposition to the ecosystem is estimated at 0.1147 kg N ha⁻¹ yr⁻¹, comprising 46% of total inorganic reactive nitrogen deposition. This is significantly lower than previous estimates for RMNP, which did not consider the bidirectionalbi-directional nature of the exchange. Due to the observed low bias in passive NH3 observations and the sensitivity The sum of simulations to NH3 concentrations, this is likely a low bound. The sensitivity of NH3 flux modelling to χ_a was tested by scaling the input concentration by 9% to account for the error discussed in Puchalski et al. (2011). This resulted in an annual reduced N deposition increase of 47%, indicating the importance of accurate NH₃ measurements for flux modelling. Additionally, since the highest NH₃ concentrations occur during upslope events, the sources contributing to these 525 events likely have a disproportionate effect on inputs (wet and dry) constitutes 60% of total N_E deposition. One limitation of this model is the exclusion of snow cover, which could significantly change NH3 fluxes in the winter, when RMNP has frequent snow events. To probe the impact of snow cover, a sensitivity test was conducted setting γ_g equal to zero during the winter (December, January, and February), which increased annual deposition by 0.06 kg N ha-1 yr-1. However, this analysis does not take into account how the surface differences may change NH3 fluxes above snow. Future works should investigate NH3 fluxes 530 above snow cover to better simulate the exchange of NH₃ in regions with snow.

Due to the cost and technical challenges of making continual, high_-time_-resolution NH₃ concentration measurements, there is growing interest in using integrated biweekly passive NH₃ measurements, such as those from the NADP AMoN network, for flux simulations. Here, we establish that a site-specific correction can be used to correct a bias introduced by using lower time_-resolution passive NH₃ measurements over the studied forest canopy in RMNP. We also establish that an average NH₃ diel pattern can be used to interpolate 30-minute NH₃ concentration and correct for the bias introduced by passive NH₃ measurements. In RMNP, a month of measurements proved sufficient to determine the diel pattern used for flux simulations. The correction factor and diel pattern, however, likely vary by location due to differences in ecosystem characteristics and

factors influencing NH₃ concentrations. Due to the potential regional differences and changes associated with land surface type, additional sites should be studied to assess the impact of measurement time-resolution on NH₃ flux simulations. To understand the seasonal variability in diel pattern and efficacy of diel pattern application for flux simulations, measurements should be conducted for a full year.

Local micrometeorological and soil measurements are also frequently unavailable, making the use of reanalysis data a desirable alternative for NH₃ flux simulations. In our location, the use of reanalysis data adds a bias that leads to overestimates of net NH₃ deposition. We found it was possible to apply a correction to address this bias, but this factor likely varies by location, in particular over different land surface types within a reanalysis grid cell. Future studies should explore the relationship between in situ measurements and reanalysis products above different land surface types, above varied topography, and in different regions. Understanding how to correct for the biases introduced through the use of reanalysis data would allow improved modelling of NH₃ bidirectional fluxes in regions lacking high time-resolution measurements.

In this analysis, we simulated the bidirectional exchange of NH₃ above a forest ecosystem using the model proposed in Massad et al. (2010). However, there are other bidirectional exchange models (e.g., Zhang et al., 2010; Pleim et al., 2013) and their simulated fluxes may differ significantly from the model used here (Jongenelen et al., 2025). In the bidirectional exchange model used here, we observe that the selected inputs for NH₃ concentration and meteorological data may introduce biases into the simulated NH₃ fluxes. This may also be true for the other models when simulating NH₃ bidirectional exchange, a good topic for future research.

555 Data Availability

560

The ammonia concentration data used in the study will be published after the manuscript is accepted. The NEON flux tower eddy covariance data bundle is available at: https://data.neonscience.org/data-products/DP4.00200.001. ERA5 reanalysis data is available at: https://www.ecmwf.int/en/forecasts/dataset/ecmwf-reanalysis-v5. CASTNET data are available at: https://nadp.slh.wisc.edu/networks/national-trends-network/.

Author Contributions

JC, BS, DP, and JW designed the measurement campaign. LN, AS, and DP made and processed Rocky Mountain National Park measurements. DP developed the model code. LN designed and ran the bidirectional exchange simulations. LN prepared the manuscript with contributions from all co-authors.

565 Competing interest

The authors declare that they have no conflict of interest.

Disclaimer

The results contain modified Copernicus Climate Change Service information 2020. Neither the European Commission nor ECMWF is responsible for any use that may be made of the Copernicus information or data it contains. The results make use of data collected by the CASTNET program from the U.S. Environmental Protection Agency. The views expressed are of the authors and do not necessarily reflect those of the U.S. EPA or any other organizations that the data used was obtained from.

Acknowledgments

The authors would also like to thank the NEON team for their support in collecting biweekly passive NH₃ data. The authors thank Nikolas Tafoya for his assistance in collecting measurements on the NEON Tower.

575 Financial support

This work was supported by the U.S. Environmental Protection Agency Regional Applied Research Efforts Program, Project #2237 and the National Park Service. This material is based in part upon work supported by the National Science Foundation through the National Ecological Observatory Network Program. The NEON Program is operated under a cooperative agreement by Batelle.

580 References

Appel, K. W., Bash, J. O., Fahey, K. M., Foley, K. M., Gilliam, R. C., Hogrefe, C., Hutzell, W. T., Kang, D., Mathur, R., Murphy, B. N., Napelenok, S. L., Nolte, C. G., Pleim, J. E., Pouliot, G. A., Pye, H. O. T., Ran, L., Roselle, S. J., Sarwar, G., Schwede, D. B., Sidi, F. I., Spero, T. L., and Wong, D. C. (2021) The Community Multiscale Air Quality Model Version 5.3 and 5.3.1: System Updates and Evaluation, Geosci. Model Dev. doi: https://doi.org/10.5194/gmd-14-2867-2021

- Baron, J. S. (2006), Hindcasting Nitrogen Deposition To Determine An Ecological Critical Load, Ecological Applications, 16(2), 433-439, doi:https://doi.org/10.1890/1051-0761(2006)016[0433:HNDTDA]2.0.CO;2.
 - Baron, J. S., H. M. Rueth, A. M. Wolfe, K. R. Nydick, E. J. Allstott, J. T. Minear, and B. Moraska (2000), Ecosystem Responses to Nitrogen Deposition in the Colorado Front Range, Ecosystems, 3(4), 352-368, doi:10.1007/s100210000032.
- Beem, K. B., et al. (2010), Deposition of reactive nitrogen during the Rocky Mountain Airborne Nitrogen and Sulfur (RoMANS) study, Environmental Pollution, 158(3), 862-872, doi:https://doi.org/10.1016/j.envpol.2009.09.023.

- Benedict, K. B., C. M. Carrico, S. M. Kreidenweis, B. Schichtel, W. C. Malm, and J. L. Collett Jr (2013a), A seasonal nitrogen deposition budget for Rocky Mountain National Park, Ecological Applications, 23(5), 1156-1169, doi:https://doi.org/10.1890/12-1624.1.
- Benedict, K. B., D. Day, F. M. Schwandner, S. M. Kreidenweis, B. Schichtel, W. C. Malm, and J. L. Collett (2013b),
- Observations of atmospheric reactive nitrogen species in Rocky Mountain National Park and across northern Colorado, Atmospheric Environment, 64, 66-76, doi:https://doi.org/10.1016/j.atmosenv.2012.08.066.
 - Benedict, K. B., A. J. Prenni, A. P. Sullivan, A. R. Evanoski-Cole, E. V. Fischer, S. Callahan, B. C. Sive, Y. Zhou, B. A. Schichtel, and J. L. Collett, Jr. (2018), Impact of Front Range sources on reactive nitrogen concentrations and deposition in Rocky Mountain National Park, doi:https://doi.org/10.7717/peerj.4759.
- 600 Benish, S. E. and Bash, J. O. and Foley, K. M. and Appel, K. W. and Hogrefe, C. and Gilliam, R. and Pouliot, G. (2022) Long-term regional trends of nitrogen and sulfur deposition in the United States from 2002 to 2017, Atmospheric Chemistry and Physics, doi:https://doi.org/10.5194/acp-22-12749-2022
 - Bobbink, R. (1991), Effects of Nutrient Enrichment in Dutch Chalk Grassland, Journal of Applied Ecology, 28(1), 28-41, doi:10.2307/2404111.
- 605 Boot, C. M., E. K. Hall, K. Denef, and J. S. Baron (2016), Long-term reactive nitrogen loading alters soil carbon and microbial community properties in a subalpine forest ecosystem, Soil Biology and Biochemistry, 92, 211-220, doi:https://doi.org/10.1016/j.soilbio.2015.10.002.
 - Bowker, G.E., Schwede, D.B., Lear, G.G. et al. Quality Assurance Decisions with Air Models: A Case Study of Imputation of Missing Input Data Using EPA's Multi-layer Model. Water Air Soil Pollut 222, 391–402 (2011).
- 610 https://doi.org/10.1007/s11270-011-0832-7
 - Bowman, W. D., J. Murgel, T. Blett, and E. Porter (2012), Nitrogen critical loads for alpine vegetation and soils in Rocky Mountain National Park, Journal of Environmental Management, 103, 165-171, doi:https://doi.org/10.1016/j.jenvman.2012.03.002.
 - Butler, T., F. Vermeylen, C. M. Lehmann, G. E. Likens, and M. Puchalski (2016), Increasing ammonia concentration trends
- 615 in large regions of the USA derived from the NADP/AMoN network, Atmospheric Environment, 146, 132-140, doi:https://doi.org/10.1016/j.atmosenv.2016.06.033.
 - Burns, D. A. (2003), Atmospheric nitrogen deposition in the Rocky Mountains of Colorado and southern Wyoming—a review and new analysis of past study results, Atmospheric Environment, 37(7), 921-932, doi:https://doi.org/10.1016/S1352-2310(02)00993-7.
- 620 Colorado Department of Public Health and Environment (CDPHE), Air Pollution Control Divison (2007), Nitrogen Deposition
 Reduction Plan. Colorado Department of Public Health and Environment. available at:

 https://www.colorado.gov/pacific/cdphe/rocky-mountain-national-park-nitrogen-reduction-plan
 - Dempster, J. (2001), CHAPTER SIX Signal Analysis and Measurement, in *The Laboratory Computer*, edited by J. Dempster, pp. 136-171, Academic Press, London, doi:https://doi.org/10.1016/B978-012209551-1/50039-8.

- 625 Driscoll, C., Milford, J. B., Henze, D. K., & Bell, M. D. (2024), Atmospheric reduced nitrogen: Sources, transformations, effects, and management, Journal of the Air & Waste Management Association, 74(6), 362–415, doi:https://doi.org/10.1080/10962247.2024.2342765
 - Galloway, J. N., A. R. Townsend, J. W. Erisman, M. Bekunda, Z. Cai, J. R. Freney, L. A. Martinelli, S. P. Seitzinger, and M. A. Sutton (2008), Transformation of the Nitrogen Cycle: Recent Trends, Questions, and Potential Solutions, Science,
- 630 320(5878), 889-892, doi:10.1126/science.1136674.
 - Gebhart, K. A., B. A. Schichtel, W. C. Malm, M. G. Barna, M. A. Rodriguez, and J. L. Collett (2011), Back-trajectory-based source apportionment of airborne sulfur and nitrogen concentrations at Rocky Mountain National Park, Colorado, USA, Atmospheric Environment, 45(3), 621-633, doi:https://doi.org/10.1016/j.atmosenv.2010.10.035.
 - Giusti, M. (2024). ERA5: How to calculate Obukhov Length. Copernicus Knowledge Base. European Centre for Medium-
- Range Weather Forecasts (ECMWF).
 - https://confluence.ecmwf.int/display/CKB/ERA5%3A+How+to+calculate+Obukhov+Length
 - Hendriks, C., R. Kranenburg, J. J. P. Kuenen, B. Van den Bril, V. Verguts, and M. Schaap (2016), Ammonia emission time profiles based on manure transport data improve ammonia modelling across north western Europe, Atmospheric Environment, 131, 83-96, doi:https://doi.org/10.1016/j.atmosenv.2016.01.043.
- 640 Hersbach, H. et al. (2020). The ERA5 Global Reanalysis. Quarterly Journal of the Royal Meteorological Society, 146, 1999-2049. https://doi.org/10.1002/qj.3803
 - Hicks, B. B., D. D. Baldocchi, T. P. Meyers, R. P. Hosker, and D. R. Matt (1987), A preliminary multiple resistance routine for deriving dry deposition velocities from measured quantities, Water, Air, and Soil Pollution, 36(3), 311-330, doi:10.1007/BF00229675.
- 645 Hogrefe, C., Bash, J. O., Pleim, J. E., Schwede, D. B., Gilliam, R. C., Foley, K. M., Appel, K. W., and R. Mathur (2023), An analysis of CMAQ gas-phase dry deposition over North America through grid-scale and land-use-specific diagnostics in the context of AQMEII4, Atmos. Chem. Phys., 23, 8119–8147, https://doi.org/10.5194/acp-23-8119-2023.
 - Holtgrieve, G. W., et al. (2011), A Coherent Signature of Anthropogenic Nitrogen Deposition to Remote Watersheds of the Northern Hemisphere, Science, 334(6062), 1545-1548, doi:10.1126/science.1212267.
- 650 Hu, C., Griffis, T. J., Frie, A., Baker, J. M., Wood, J. D., Millet, D. B., et al. (2021), A multiyear constraint on ammonia emissions and deposition within the US Corn Belt. Geophysical Research Letters, 48, e2020GL090865. https://doi.org/10.1029/2020GL090865https://doi.org/10.1029/2020GL090865
 - Jongenelen, T., M. van Zanten, E. Dammers, R. Wichink Kruit, A. Hensen, L. Geers, and J. W. Erisman (2025), Validation and uncertainty quantification of three state-of-the-art ammonia surface exchange schemes using NH3 flux measurements in a dune ecosystem, *Atmos. Chem. Phys.*, 25(9), 4943-4963, doi:10.5194/acp-25-4943-2025.
- Juncosa Calahorrano, J. F., Sullivan, A. P., Pollack, I. B., Roscioli, J. R., McCabe, M. E., Steinmann, K. M., Caulton, D. R., Li, E., Pierce, J. R., Naimie, L. E., Pan, D., Collett, J. L., Jr, & Fischer, E. V. (2024), Anatomy of Summertime Upslope Events

Formatted: Check spelling and grammar, Subscript

- in Northeastern Colorado: Ammonia (NH₈) Transport to the Rocky Mountains. Environmental science & technology, 58(38), 16922–16930. https://doi.org/10.1021/acs.est.3c10902
- 660 Kanakidou, M., S. Myriokefalitakis, N. Daskalakis, G. Fanourgakis, A. Nenes, A. R. Baker, K. Tsigaridis, and N. Mihalopoulos (2016), Past, Present, and Future Atmospheric Nitrogen Deposition, Journal of the Atmospheric Sciences, 73(5), 2039-2047, doi:https://doi.org/10.1175/JAS-D-15-0278.1.
 - Korb, J. E., and T. A. Ranker (2001), Changes in stand composition and structure between 1981 and 1996 in four Front Range plant communities in Colorado, Plant Ecology, 157(1), 1-11, doi:10.1023/A:1013772220131.
- 665 Li, Y., B. A. Schichtel, J. T. Walker, D. B. Schwede, X. Chen, C. M. B. Lehmann, M. A. Puchalski, D. A. Gay, and J. L. Collett (2016), Increasing importance of deposition of reduced nitrogen in the United States, Proceedings of the National Academy of Sciences, 113(21), 5874-5879, doi:10.1073/pnas.1525736113.
 - Massad, R. S., E. Nemitz, and M. A. Sutton (2010), Review and parameterisation of bi-directional ammonia exchange between vegetation and the atmosphere, Atmos. Chem. Phys., 10(21), 10359-10386, doi:10.5194/acp-10-10359-2010.
- 670 Meyers, T. P., Finkelstein, P., Clarke, J., Ellestad, T. G., & Sims, P. F. (1998). A multilayer model for inferring dry deposition using standard meteorological measurements. Journal of Geophysical Research, 103(D17), 22645–22661.
 - Montes, F., C. A. Rotz, and H. Chaoui (2009). Process Modeling of Ammonia Volatilization from Ammonium Solution and Manure Surfaces: A Review with Recommended Models. Transactions of the ASABE, 52(5), 1707-1720, doi:https://doi.org/10.13031/2013.29133.
- National Atmospheric Deposition Program (NRSP-3). 2022. NADP Program Office, Wisconsin State Laboratory of Hygiene, 465 Henry Mall, Madison, WI 53706.
 - NEON (National Ecological Observatory Network). Site management and event reporting (DP1.10111.001), RELEASE-2023. https://doi.org/10.48443/9p2t-hj77. Dataset accessed from https://data.neonscience.org/data-products/DP1.10111.001/RELEASE-2024 on September 05, 2023.
- 680 Nemitz, E., C. Milford, and M. A. Sutton (2001), A two-layer canopy compensation point model for describing bi-directional biosphere-atmosphere exchange of ammonia, Quarterly Journal of the Royal Meteorological Society, 127(573), 815-833, doi:https://doi.org/10.1002/qj.49712757306.
 - Pan, D., et al. (2021), Ammonia Dry Deposition in an Alpine Ecosystem Traced to Agricultural Emission Hotpots, Environmental Science & Technology, 55(12), 7776-7785, doi:10.1021/acs.est.0c05749.
- 685 Pan, Y., et al. (2020), Systematic low bias of passive samplers in characterizing nitrogen isotopic composition of atmospheric ammonia, Atmospheric Research, 243, 105018, doi:https://doi.org/10.1016/j.atmosres.2020.105018.
 - Pleim, J. E., J. O. Bash, J. T. Walker, and E. J. Cooter (2013), Development and evaluation of an ammonia bidirectional flux parameterization for air quality models, Journal of Geophysical Research: Atmospheres, 118(9), 3794-3806, doi:https://doi.org/10.1002/jgrd.50262.

- 690 Puchalski, M. A., M. E. Sather, J. T. Walker, C. M. B. Lehmann, D. A. Gay, J. Mathew, and W. P. Robarge (2011), Passive ammonia monitoring in the United States: Comparing three different sampling devices, Journal of Environmental Monitoring, 13(11), 3156-3167, doi:10.1039/C1EM10553A.
 Schiferl, L. D., Heald, C. L., Van Damme, M., Clarisse, L., Clerbaux, C., Coheur, P.-F., Nowak, J. B., Neuman, J. A., Herndon,
 - Schiferi, L. D., Heald, C. L., Van Damme, M., Clarisse, L., Clerbaux, C., Coheur, P.-F., Nowak, J. B., Neuman, J. A., Herndon, S. C., Roscioli, J. R., and Eilerman, S. J. (2016), Interannual variability of ammonia concentrations over the United States:
- 695 sources and implications, Atmos. Chem. Phys., 16, 12305–12328, doi:https://doi.org/10.5194/acp-16-12305-2016.
 Schrader, F., M. Schaap, U. Zöll, R. Kranenburg, and C. Brümmer (2018), The hidden cost of using low-resolution concentration data in the estimation of NH₃ dry deposition fluxes, Scientific Reports, 8(1), 969, doi:10.1038/s41598-017-
 - Schwede, D. B., and G. G. Lear (2014), A novel hybrid approach for estimating total deposition in the United States,
 - Shen, J., D. Chen, M. Bai, J. Sun, T. Coates, S. K. Lam, and Y. Li (2016), Ammonia deposition in the neighbourhood of an intensive cattle feedlot in Victoria, Australia, Scientific Reports, 6(1), 32793, doi:10.1038/srep32793.
 - Stratton, J. J., J. Ham, and T. Borch (2018), Ammonia Emissions from Subalpine Forest and Mountain Grassland Soils in Rocky Mountain National Park, Journal of Environmental Quality, 47(4), 778-785,
- 705 doi:https://doi.org/10.2134/jeq2018.01.0023.

18021-6.

- Stull R B (1988) An Introduction to Boundary Layer Meteorology; Kluwer Academic, Dordrecht, doi: https://doi.org/10.1007/978-94-009-3027-8.
- Sutton, M. A., J. K. Schjørring, G. P. Wyers, J. H. Duyzer, P. Ineson, D. S. Powlson, D. Fowler, D. S. Jenkinson, J. L. Monteith, and M. H. Unsworth (1995), Plant—atmosphere exchange of ammonia, Philosophical Transactions of the Royal Society of
- 710 London. Series A: Physical and Engineering Sciences, 351(1696), 261-278, doi:doi:10.1098/rsta.1995.0033.

Atmospheric Environment, 92, 207-220, doi:https://doi.org/10.1016/j.atmosenv.2014.04.008.

- Tanner, E., N. Buchmann, and W. Eugster (2022), Agricultural ammonia dry deposition and total nitrogen deposition to a Swiss mire, Agriculture, Ecosystems & Environment, 336, 108009, doi:https://doi.org/10.1016/j.agee.2022.108009.
- Thom, A. S. (1975), Momentum, mass and heat exchange of plant communities. Vol.1, Edited by J.L. Monteith, London.
- Tomsche, L., et al. (2023), Measurement report: Emission factors of NH3 and NHx for wildfires and agricultural fires in the
- 715 United States, Atmos. Chem. Phys., 23(4), 2331-2343, doi:10.5194/acp-23-2331-2023.
 - U.S. Environmental Protection Agency Clean Air Markets Division (2024 b), Clean Air Status and Trends Network (CASTNET), [Weekly Dry Deposition], Available at www.epa.gov/castnet, Date accessed: [02 20, 2024]
 - U.S. Environmental Protection Agency Clean Air Markets Division (2024b), Clean Air Status and Trends Network (CASTNET), [Weekly Filter Pack], Available at www.epa.gov/castnet, Date accessed: [02 20, 2024]
- 720 U.S. Environmental Protection Agency, National Emissions Inventory [Tier I CAPS] (2023), available via https://www.epa.gov/air-emissions-inventories/national-emissions-inventory-nei. Accessed June 05, 2024.

Formatted: Check spelling and grammar, Subscript

Formatted: Check spelling and grammar, Subscript

- Walker, J. T., P. Spence, S. Kimbrough, and W. Robarge (2008), Inferential model estimates of ammonia dry deposition in the vicinity of a swine production facility, Atmospheric Environment, 42(14), 3407-3418, doi:https://doi.org/10.1016/j.atmosenv.2007.06.004.
- Walker, J. T., et al. (2019a), Toward the improvement of total nitrogen deposition budgets in the United States, Science of The Total Environment, 691, 1328-1352, doi:https://doi.org/10.1016/j.scitotenv.2019.07.058.
 - Walker, J. T., M. D. Bell, D. Schwede, A. Cole, G. Beachley, G. Lear, and Z. Wu (2019b), Aspects of uncertainty in total reactive nitrogen deposition estimates for North American critical load applications, Science of The Total Environment, 690, 1005-1018, doi:https://doi.org/10.1016/j.scitotenv.2019.06.337.
- 730 Wentworth G. R., Murphy J. G., Benedict K. B., Bangs E. J., Collett Jr J. L. (2016), The role of dew as a night-time reservoir and morning source for atmospheric ammonia. Atmospheric Chemistry and Physics. 2016;16:7435–7449. doi: 10.5194/acp-16-7435-2016.
 - Wichink Kruit, R. J., M. Schaap, F. J. Sauter, M. C. van Zanten, and W. A. J. van Pul (2012), Modeling the distribution of ammonia across Europe including bi-directional surface-atmosphere exchange, Biogeosciences, 9(12), 5261-5277,
- 735 doi:10.5194/bg-9-5261-2012.
 - Xiu, A., and J. E. Pleim (2001), Development of a Land Surface Model. Part I: Application in a Mesoscale Meteorological Model, Journal of Applied Meteorology, 40(2), 192-209, doi:https://doi.org/10.1175/1520-0450(2001)040<0192:DOALSM>2.0.CO;2.
 - Zhan, X., et al. (2017), Evidence for the Importance of Atmospheric Nitrogen Deposition to Eutrophic Lake Dianchi, China,
- 740 Environmental Science & Technology, 51(12), 6699-6708, doi:10.1021/acs.est.6b06135.
 - Zhang, L., J. R. Brook., and R. Vet (2003), A revised parameterization for gaseous dry deposition in air-quality models, Atmos. Chem. Phys., 3, 2067–2082, doi:https://doi.org/10.5194/acp-3-2067-2003.
 - Zhang, L., L. P. Wright, and W. A. H. Asman (2010), Bi-directional air-surface exchange of atmospheric ammonia: A review of measurements and a development of a big-leaf model for applications in regional-scale air-quality models, Journal of
- 745 Geophysical Research: Atmospheres, 115(D20), doi:https://doi.org/10.1029/2009JD013589.